SLAC-PUB-1981
July 1977
(E)

PRODUCTION OF MUON PAIRS IN K_L^o - Cu INTERACTIONS†

M. Faessler*, J. Kirkby, J. Liu,** S. Wojcicki

Stanford Linear Accelerator Center

and

Physics Department

Stanford University
Stanford, California 94305

R. Burns, P. Condon, P. Cowell

University of California
Irvine, California 92664

ABSTRACT

The di-muon production mass spectrum has been measured with a beam of 4-20 GeV/c K_L^o's incident on a copper target. The production of μ-μ pairs resulting from the decay of vector mesons, (ρ, ω, and ϕ) was observed with a cross section of 2.4 mb based on a specific production model. Upper limits of 2.9 μb and 90 nb are placed on the production cross sections for ψ(3100) and anomalous low mass ($m_{\mu\mu}$ < 0.5 GeV/c^2) di-muons respectively.

†Work supported in part by the Energy Research and Development Administration.
*Current address: CERN, Geneva, Switzerland
**Presently with American Asian Bank, San Francisco, California

(Submitted to Phys. Rev.)

I. INTRODUCTION

The first observation of direct muons in hadronic interaction took place almost 10 years ago in an experiment by Leon Lederman and his collaborators.[1] We use the word "direct muons" to denote those muons which do not come from such conventional processes as π, K, or hyperon decay, or Bethe-Heitler conversions of photons into muon pairs in the target material. The search for muons was motivated at that time[2] principally by the fact that a high P_T muon might be a signature of intermediate vector boson production in hadronic processes, i.e.

$$p^+ p \rightarrow W^\pm + \text{hadrons},$$

followed by

$$W^\pm \rightarrow \mu^\pm + \nu_\mu \quad .$$

It was pointed out subsequently by Yamaguchi[3] that the production of W bosons must be related by CVC to the production of heavy virtual photons, which could subsequently decay to muon pairs. Thus the presence of the $\gamma^* \rightarrow \mu^+\mu^-$ process would obscure the interpretation of any possible observed high P_T muon signal in hadronic interactions.

More recently the question of direct muons received an added stimulus on both the theoretical and experimental fronts. On the theoretical side, a calculation of the hadron constituent annihilation process by Drell and Yan[4] indicated that this cross section is surprisingly large. Shortly afterwards, both direct muons and electrons were observed in hadronic interactions at Fermilab at intermediate and high P_T, with a lepton/pion ratio pretty much constant at about 10^{-4} over a wide range of P_T and incident energies.[5] The observed rate was surprisingly large and could not be accounted for either by the more conventional mechanism like the vector meson production followed by decay into lepton pairs or the Drell-Yan mechanism with the conventional parton distribution. The subsequent discovery of ψ[6] and ψ'[7] with their high electromagnetic decay rate provided another possible source of direct leptons, especially at high P_T's. The subsequently measured ψ and ψ' production cross sections in hadronic interactions were also, however, considerably too low to account for all the observed direct leptons.[8]

This excess of direct muons was especially intriguing in light of strong theoretical arguments for the existence of particles with a new flavor named charm[9] needed to explain the absence of the decay mode $K_L^o \rightarrow \mu^+\mu^-$ at any appreciable rate.[10] These particles would have to decay weakly on a time scale of $\sim 10^{-13}$ sec and could have appreciable leptonic and semileptonic decay rates, thus providing the needed source of direct leptons. Of course, aside from any specific theoretical models, direct leptons could be evidence for the production of a whole variety of new particles with weak decay modes, such as hadrons with new quantum members or heavy leptons.

More recently, Farrar and Frautschi[11] pointed out that the existing data were not incompatible with a copious (1-10% of pions) production of single photons which subsequently gave rise to the observed leptons.

The electromagnetic, as opposed to weak, origin of direct leptons in hadronic interactions received support recently from the two experiments at Fermilab comparing their dimuon yields with the total single muon yield.[12] The results of the comparison indicated that at Fermilab energies the total single muon production rate was consistent with coming solely from the dimuon pairs. On the other hand, a contribution at the level of 20-25% from sources other than dimuons could not be excluded.

A contradictory conclusion was reached by a group working at lower energies at Serpukhov who found a μ^+/μ^- ratio of 1.21,[13] thus indicating presence of muons from sources other than electromagnetic.

There have also been performed two sets of experiments on muon polarization, which yielded contradictory results. The Yale group working at Fermilab found polarization consistent with zero,[14] both at low P_T's and at a mean P_T of 2.15 GeV/c. Thus these results support the conclusion they have reached from the study of production rates, namely that the majority of the muons are of electromagnetic origin. The Serbukhov group, however, found a non-zero polarization at high P_T's,[15] consistent with the dominant source being a weak decay of a new hadron via a V + A current.

Since the initial pioneering work on direct lepton production, a variety of other groups have either performed new experiments that explored this production process in different P_T and s ranges,[16] or reanalyzed the old experiments to extract the prompt lepton signals.[17] The subject is too extensive to be covered adequately here; the interested reader can be referred to many excellent review talks on this subject.[18] We shall limit ourselves here only to pointing out some of the salient features of the overall situation.

Even though most of the experiments are in reasonably good agreement with each other there are some contradictory results which make even the experimental situation slightly obscure. On the whole, however, one can say that generally the lepton-pion ratio is $\sim 10^{-4}$ over a wide range of kinematical variables, with a falloff as one goes to high x values. In addition, there are strong indications that the e/π ratio increases as we go to lower P_T's.[19]

There is some experimental uncertainty at present as to whether a threshold exists for the direct lepton production,[20] with the comparison of different experiments made more difficult by the fact that generally different kinematical regions are investigated in different experiments.

Since the discovery of charmed particles[21] and the observation of their semileptonic (or possibly purely leptonic) decay modes in both the neutrino[22] and the e^+e^- colliding beam[23] experiments, it appears clear that some of the direct leptons in hadronic collisions must come from the charmed particle decays. So far, however, all the direct searches for charmed particles in hadronic interactions have turned out to be negative,[24] so the magnitude of the level of this contribution remains a wide open question.

This experiment attempts to answer the question as to whether muon pairs, other than from known particle decays, are produced in the K^o interactions in the intermediate energy range. The necessity of looking for muon pairs as opposed to single muons is dictated almost exclusively by the prohibitively large background of single muons due to π and K decay.

II. APPARATUS

The experiment was carried out at the Stanford Linear Accelerator Center using a modified version of the K_L^o Spectrometer Facility as shown in Fig. 1. A total of 7 absorption lengths (λ) of Cu, consisting of 14 slabs of Cu, each 80 cm x 40 cm x 7.5 cm, was positioned in the path of the K_L^o beam which itself was 60 cm x 30 cm in area. The first interaction length of Cu represented the target, while the next 6 constituted the front hadron absorber. The first 4 slabs in this assembly were movable along the beam direction, allowing us to vary the effective density of that portion of the target-absorber material which was most significant from the point of view of pion decays. We ran with 0, 4, and 8 cm air gaps between these slabs, and shall refer to these data as 0, 4, and 8 cm data. Additional Pb shielding was stacked around the Cu absorber to cut down the wide-angle hadrons.

A 75 cm x 45 cm veto counter V was placed about 2m upstream of the target to define the decay region for $K^{o}_{\mu 3}$ decays. When accompanied by the subsequent decay $\pi \rightarrow \mu\nu$ these events provided the flux measurement for the experiment. The downstream limit of the decay region was defined by two banks of scintillation counters P and Q, each composed of 6 horizontal counters of dimension 60 cm x 5 cm x 0.3 cm. A similar horizontal bank R and a 13-counter vertical bank S were positioned between the Cu target and the absorber, and a 17-counter vertical bank T was placed behind the Cu absorber. Both the S and T counters were of the same size as the P, Q, and R counters. The T counter bank was followed by 10 planes (4X, 4Y, U and V) of capacitive-readout wire spark chambers, followed by a 100D40 dipole analyzing magnet. The magnetic field was constantly monitored by an NMR probe and had a typical $\int Bdl$ value of 12.6 kG-m. Two separate groups of wire chambers, each consisting of 2X and 2Y readout planes, were arranged behind the magnet in such a way as to cover the maximum solid angle. A bank of 23 vertical 15 cm x 168 cm x 1.25 cm A counters were positioned before a 2.5 λ Pb absorber, followed by a similar bank of 25 vertical B counters. Behind the B's on one side of the spectrometer were 2 large wire chambers which were used to measure the X and Y coordinates of muons which penetrated the Pb wall. These will be referred to as the "muon WSC's."

The V counter was viewed by two 56AVP phototubes at each end, while the P, Q, R, S, and T counters each had a single 56AVP phototube. The A and B counters were viewed by XP1021 and 56AVP phototubes respectively, one at each end of a counter. The anode signal from each phototube was discriminated and the discriminator output fed into both latch and time-of-flight (TOF) circuits, the latter having a typical sensitivity of 0.1 nsec/channel. In addition, all the discriminator outputs from each bank of counters were mixed to form overall trigger levels for each counter bank separately. Both the latch and TOF gates were generated by the output of the A mixer.

The experiment was run using a 3 mA primary SLAC electron beam of 21.5 GeV, with a neutral beam extracted at 1.5 degrees off a 1 rl Be target. In order to cut down the direct gamma component in this beam, 58 rl of Pb were placed in the beam before the first collimator. Likewise, in order to improve the K_L^o to neutron ratio, 1.5 collision lengths of polyethylene were introduced just after the Pb absorber. Two sweeping magnets in the beam line eliminated charged particles from the beam. The K_L^o spectrum at the spectrometer is shown in Fig. 2. A total flux of 5.6 x 10^9 K_L^o was obtained during the experiment.

III. DATA ACQUISITION

Candidates for muons were required to traverse both the upstream Cu absorber and the downstream Pb absorber. Consequently, a 2T.2A.2B trigger was set up to select events with 2 muons in the final state. The three general classes of events of interest that satisfied this trigger were:

1) Interaction events in which the K_L^o interacted in the Cu target resulting in the production of 2 muons. This category of events was composed of triggers satisfying a $\bar{V}.\bar{P}.\bar{Q}.R.S.2T.2A.2B$ logic requirement.

2) $K_{\mu 3}^o$ decay events in which the $K_L^o \rightarrow \pi\mu\nu$ decay occurred in the decay region

between V and P, followed by a subsequent $\pi \rightarrow \mu\nu$ decay. These decays were defined as events satisfying a $\overline{V}$.P.Q.R.S.2T.2A.2B requirement.

3) Upstream decays in which the $K^{o}_{\mu 3}$ decay occurred upstream of the veto counter. These events satisfied a V.P.Q.R.S.2T.2A.2B requirement.

In addition, an alternate single-muon trigger V.T.A.B was also set up to record events with a single upstream muon.

When an event trigger was satisfied, the latch, ADC, and wire chamber data were all written onto a magnetic tape for subsequent off-line analysis. In addition, the on-line PDP-9 computer was used to accumulate and display numerous running histograms in order to pinpoint any malfunctions to the experimenter.

The performance of all the counters was monitored every 24 hours via LED's embedded in each of the counters. These LED runs were also used to provide calibration of each ADC unit. A single-muon run was then taken with the sweeping magnets off, thus allowing direct muons from the primary target to enter the apparatus. These runs were used to set the zero times for each ADC unit. The performance of the wire spark chambers was also closely monitored throughout the experiment and typical multi-spark efficiencies well in excess of 90% were observed in all the planes.

IV. DATA REDUCTION

A standard data-reduction technique was employed to reduce the massive amount of data acquired during the experiment to summaries on data-summary tapes of relevant information for good events. Firstly, all the found front and rear track segments were matched to form full tracks from which the track momenta were determined. A match was defined as satisfactory if the front and rear segments came together at the midplane of the magnet within 7 cm. Each full track was then checked to see if it satisfied a muon candidate criteria. As previously indicated, a minimum requirement for a muon track was that it triggered R.S.T.A.B. Subsequently, the front and rear segments of each muon candidate were projected to the various counter banks and cuts were made for X and Y positions where appropriate. For example, at the A bank the projected position was compared with the X value of the center of the nearest A counter which fired, and with the Y in that counter, as indicated by the difference in the TOF readings in the phototubes at either end of the counter. Expected X and/or Y deviations for each counter bank were determined experimentally as a function of track momentum, and these values were used as standard deviations to compute a contribution to an overall muon χ^2 at each counter bank. In addition, a minimum residual kinetic energy of 0.1 GeV was required of all the muon candidates as they left the downstream end of the Pb filter.

The TOF readings from the A and B counters associated with a muon candidate were averaged to give a reference time for that muon candidate. The TOF readings of corresponding counters in all other banks, after corrections for position in the counter, were compared to this reference time. Again, a momentum-dependent σ was obtained from the data for each counter bank and contributions to the muon χ^2 were computed for each counter bank. The overall muon χ^2 thus consisted of two components, one from the geometrical comparison and one from the TOF comparison.

For the muon candidate to be accepted as a muon for the subsequent analysis it had to have a $\chi^2 < 30$ or 40 depending whether it was an interaction

$(\bar{V}.\bar{P}.\bar{Q}.R.S.T.A.B)$ or decay $(P.Q.R.S.T.A.B)$ muon. The difference in the cutoff compensated for the extra contribution to the χ^2 of the P and Q counters necessary for the decay muons.

An average muon time for each muon track was derived by weighting the corrected TOF reading in each associated counter by $1/\sigma^2$, where σ was the appropriate standard deviation for that particular counter bank.

From the Fermi formula for multiple scattering,[25] it can be shown that the best estimate for the initial direction of a muon is

$$\hat{u} = 1/2(3\hat{u}_{proj} - \hat{u}_{meas}) \quad ,$$

where $\hat{u}_{meas}$ is the measured direction in the front wire spark chambers, and $\hat{u}_{proj}$ is defined by the exit position of the track at the end of the Cu absorber and the location of the best-estimated interaction or decay point. For all muons, and X and Y of this production point were determined from the location of the associated P, Q, R, and S counters. The Z location of the origin of interaction and decay muons was taken to be the mean Z for interactions and decays respectively, while that for the upstream muons was taken to be 50 cm in front of the veto counter.

The analysis program then proceeded to find all vertices between pairs of good muon tracks, using the best-estimate muon directions. Fig. 3 shows the distribution in d^2, the square of the distance of closest approach between pairs of muon tracks in the final K decay data sample, together with the expected distribution calculated by a Monte Carlo technique. In addition, all possible vertices between a full track, not necessarily a muon, and an unmatched front track segment were also calculated for subsequent use in background subtraction (see below).

Finally, the candidates for good decay or interaction events were defined by the following criteria:

1) two good full muon tracks,

2) $|\mathrm{TOF}\ (\mu^+) - \mathrm{TOF}\ (\mu^-)| \leq 1.2$ nsec,

3) satisfactory vertex, with $d^2 < 225\ \mathrm{cm}^2$.

The events passing these tests formed the raw sample of interaction, decay, or upstream decay candidates. The number of events in each of the three categories at this stage is enumerated in Table I.

V. MONTE CARLO

A Monte Carlo simulation of the experiment was performed in order to determine the detection efficiency of the apparatus as a function of the mass of the produced di-muon/pair, as well as the efficiency for $K^o_{\mu 3}$ decays. The differential cross section for $K^o_L + N \to \mu^+\mu^- X$ was taken to have the form

$$\frac{d^2\sigma}{dx\ dP_T^2} \propto (1 - |x|)^3\ e^{-4.2\ P_T^2}\ , \qquad (\mathrm{V.1})$$

where $x = P^*_{/\!/}/P^{*\ max}_{/\!/}$, and P_T is the transverse momentum of the $\mu^+\mu^-$ pair. This form was able to reproduce reasonably well the observed P_T and E distribution of the di-muon pairs in the vector meson region, as illustrated in Fig. 4 where the actual data is compared with the Monte Carlo prediction. The relative efficiency of the spectrometer as a function of di-muon mass is shown in Fig. 5. The calculated probability of the occurrence and detection of the process

$$K^o_L \to \pi\mu\nu\ ,\ \pi \to \mu\nu$$

was 3.7×10^{-7} per incident K_L^o averaged over the momentum spectrum of the incident beam.

The form factors for $K_{\mu 3}^o$ decay were taken from Donaldson et al.[26] Full accounting of multiple scattering and ionization energy loss was included in the Monte Carlo. The accepted events were subjected to a similar set of cuts as were applied to the data.

VI. BACKGROUND SUBTRACTION

Whereas the raw samples of K decays and upstream K decays are already relatively pure, a sizable fraction of the interaction events involve a pair of "μ's" which originated near the downstream end of the Cu absorber. The two main processes that contribute here are:

a) A K_L^o interaction which triggers the R and S counters occurring accidentally in time with an interaction or decay of another K_L^o near the downstream end of the absorber. The probability that a 1 GeV π produced at the end of the Cu block will register as a μ is a non-negligible 12%. It can do so either by decaying in the 4 m of He in the magnet, or by punching through the 46 cm of Pb between the A and B counters.

b) A single K_L^o first undergoes an interaction in the Cu target, leaving there a small part of its energy but enough to trigger R and S. The same K_L^o then penetrates almost to the end of the Cu absorber before interacting again or decaying. It is the products of this decay or second interaction which give rise to the 2 μ's which pass all subsequent cuts.

The sizable contribution due to these two sources to the "interaction events" is illustrated in Fig. 6 where we display the Z distribution of the vertex point for the three categories of accepted events. Whereas the two decay categories exhibit the expected distributions, the interaction events show an excess of events near the downstream end of the absorber, indicating the presence of the background discussed above. Additional evidence for this kind of background comes from the visual inspection of the events. Whereas the decay events tend to be rather clean with essentially no extraneous sparks aside from the ones associated with the two muons, a certain subset of the interaction events show a high multiplicity of tracks pointing to a location just inside the Cu absorber.

The interaction sample can be greatly purified by eliminating those events where at least one pair of (full + full) or (full + unmatched front) tracks gave a "very good" intersection near the end of the Cu absorber, with $d^2 < 5$ cm^2 and $-260 < Z < -220$ cm. We emphasize the "very good" as opposed to merely satisfactory requirement here. A low mass di-muon system produced upstream in the target part of the absorber has a reasonable probability of giving a vertex near the downstream end of the absorber. But due to the Coulomb scattering, the distance of closest approach will tend to be rather large; on the other hand, the tracks that have been produced at the end of the copper will generally give a very good vertex. According to Monte Carlo calculation, this procedure should be 100% effective in throwing out the interactions at the end of the Cu block, without losing any of the genuine events. The number of events remaining after this cut (referred to as VEND cut in the subsequent discussion) is shown in Table II, and in Fig. 6.

There still remain several other sources of contamination:

1) pions produced in the target which simulated muons either by decaying before interacting, or by penetrating the whole length of the absorber.

2) pions simulating muons (or genuine muons) produced downstream of the R and S counters which have not been eliminated by the VEND cut, but which satisfied muon selection criteria by one of the two mechanisms discussed above. In order to pass the VEND cut, these events will in general be either very low multiplicity events produced near the end of the copper or else K_L^o interactions in the middle of the copper.

3) events with each of the muons coming from a different K_L^o interaction, the two interactions being accidentally in time. The rough magnitude of this contamination can be obtained by inspecting the Δ TOF distribution for both the like sign and the unlike sign muons, shown in Fig. 7. It is apparent from Fig. 7 that a large fraction of the like sign dimuons do indeed originate from this source.

The first and third sources of contamination can be studied by looking at the like-sign di-muons and by studying the rate as a function of target density. The second source can be studied by looking at those events which did not give a P, Q, R, or S counter latch. These are presumably events due to K_L^o interactions downstream of the R and S counter banks.

We discuss first the second contamination, since that mechanism can also contribute to the like-sign dimuons. We make the assumption that the energy spectrum of the K_L^o's satisfying our "interaction event" criteria is the same whether R and S counters registered or not. This is rigorously true if the R and S counters were struck by secondaries from an interaction involving some other K_L^o. We believe it to be a reasonably good assumption even for vents where the K_L^o's lost some of their energy by undergoing a "soft" interaction in the target before producing "μ's" at the end of the copper block.

At any rate, the adopted procedure is not very sensitive to the momentum spectrum.

Based on that assumption, the ratio of the number of events eliminated by the VEND cut to those which pass the VEND cut, but occur downstream of the RS counters, is the same regardless of whether an R and S counter fired or not. Thus we processed all of the events which had neither an R or S counter ($\overline{RS}$ data) in the same manner as those which did (RS data). Subsequently we subtracted from the RS interaction events the number of $\overline{RS}$ interaction events scaled by the ratio of events eliminated by the VEND cuts in the RS and $\overline{RS}$ data samples. The results of this background subtraction are indicated in Table III where the data have been separated into the low and high di-muon mass samples.

We turn next to the discussion of the other two background sources. The yield of interaction events corrected for detection efficiency and normalized to the K_L^o flux (as obtained from $K_{\mu 3}^o$ decays) is shown in Fig. 8 as a function of density for the 0, 4, and 8 cm data. The decay contamination should increase as $(1/\rho)^2$. No evidence for any significant contribution due to decays is seen, as could have been argued "a priori" from the known $\pi^{\pm}$ and $K^{\pm}$ decay lifetimes.

It is therefore reasonable to assume that the like-sign muons have the pion punchthrough process as their main source, or else are due to accidental time coincidences. Furthermore, this same mechanism must also contribute to the unlike-sign muons. At high energies, where the multiplicities are large, it is probably a reasonable assumption to take the number of unlike-sign muons due to these sources as equal to the number of like-sign muons. On the other hand, at our low energies and the resultant low multiplicities, the most reasonable assumption is that the punchthrough's will be due mainly to π's and K's, since protons tend to be emitted at low energies in the laboratory. Table IV lists the relative numbers of + -, ++, and -- meson pairs that can be produced in 3- and 4-body K^oN reactions, on the assumption that within each class all the channels are produced with equal probability. The much higher a priori probability of having 2 unlike-sign mesons as opposed to 2 like-sign mesons is quite apparent. Thus it appears imperative to deduce the ratio of like-sign to unlike-sign punchthrough's from the experimental data itself.

To this end, we again use the $\overline{RS}$ data. Ideally one should extrapolate the ratio of unlike to like-sign dimuons as a function of Z to the position of the target. Within our statistics and resolution this ratio appears constant as a function of Z with a value of about 2.5. We therefore used this factor to multiply the number of like-sign muon events to obtain the contamination among the unlike-sign muons due to π punchthroughs and accidental time coincidences. The results of this subtraction are incorporated in Table III (c). It should be emphasized here that the subtractions in Table III(b) and (c) was performed on a mass bin basis, to allow for the different amount of each kind of contamination in each mass bin. The final mass plot resulting from our selection procedure after the above described background subtraction is illustrated in Fig. 9.

VII. DISCUSSION OF THE MASS PLOT

The inspection of the mass plot illustrated in Fig. 9 exhibits clearly the fact that the events group themselves into two categories: 1) the low mass di-muons with $m_{\mu\mu} < 0.5$ GeV/c^2, and 2) the di-muons presumably coming from the decay of the vector mesons. Furthermore, the backgrounds discussed in VI affect the low mass part of the spectrum more than the high mass (vector meson decay) region. The low mass part of the spectrum is thus more sensitive to any uncertainties in the background subtraction. Accordingly, in this section we discuss some of the experimental tests which lead us to believe that the low mass events are indeed genuine, and not some artifact of the uncertainties in the background subtraction.

One test of whether the so-called low-mass di-muon events are really due to genuine muons is the distribution of the deviations in the muon WSC's of the observed hits from the predicted hits, the latter based on extrapolating the original momentum vector downstream of the magnet through the lead absorber to the muon WSC's. This distribution, corrected for momentum dependence is displayed in Fig. 10 for the high mass events, K decays (both upstream and downstream of the V counter), residual events (after VEND cut) from the $\overline{RS}$ data, and the low mass events remaining after the background subtraction. As can be seen from Fig. 10c, which contains large amount of pion punchthrough's, this distribution is quite sensitive to the presence of any non-muon background. The similarity between Fig. 10d and Fig. 10a and 10b leads us to believe that the low mass di-muons represent a relatively pure sample.

We can perform a similar kind of comparison using now the TOF difference between the two muons, as shown in Fig. 11. Again, the conclusion is that the low mass interaction events appear to be genuine.

A possible source of spurious low mass events can be the K_L^o decays. The contribution due to "rational" K_L^o decays, i.e. those occurring between the P and R counters, is calculated in the next section. We would like to discuss here the possibility of K_L^o decays occurring upstream of the P counter, failing to register in both the P and Q counters, and thus simulating the low mass interaction events. There are two independent ways to show that this contamination is indeed negligible. We can first estimate the P and/or Q inefficiency by seeing what fraction of time the P misses when Q, R, S are present, or alternatively Q misses when P, R, S are present. These numbers are given in Table V together with the calculated probability that both P and Q miss. This calculated inefficiency leads to an expected background of 1 event, a result that is not surprising when one recalls that 2 charged particles are produced in each K_L^o decay. An independent test of the smallness of this contamination is obtained by counting the number of events with $V.\overline{P.Q}.R.S$. The observed number of 17 is perfectly consistent with the calculated number of 18 obtained from the measured V singles rate.

On the basis of the tests discussed in this section, it appears to us highly unlikely that more than 25% of the low mass di-muons could be due to sources other than genuine events occurring in the Cu target.

VIII. INTERPRETATION OF THE MASS PLOT

The most natural interpretation of the high mass ($m_{\mu\mu}$ > 0.5 GeV/c^2) spectrum is in terms of the three well known vector mesons: ρ, ω, and ϕ. Our resolution is insufficient to resolve the ρ-ω and ϕ peaks. Figure 12a indicates the Monte Carlo calculated distributions expected for pure ω, ρ, and ϕ production, arbitrarily normalized to the same production cross section times branching ratio into μ pairs. For comparison, Fig. 12b shows the expected di-muon spectrum resulting from K decays superimposed on the actual distribution. The fair agreement of the two illustrates the level of our understanding of the resolution. Finally, Figure 12c illustrates the comparison of several different mixtures of the ρ, ω, and ϕ mesons with the actual high mass data.

The presence of low mass di-muon events in hadronic events has been somewhat of a mystery during the last few years. We would like to discuss next to what extent in our experiment a new source is necessary to account for these dimuons, or whether they can be accounted by more conventional sources, like K decays in the Cu target, Bethe-Heitler pairs, or radiative decays of η and ω.

A. <u>K Decays</u>

A certain number of K_L^o's will decay in the Cu target between the Q and R counters, and will be followed either by a pion decay before its interaction or by a pion punchthrough. The calculation here is quite straightforward. We start off by calculating the relative number of K decays at each density, corrected both for the slightly different detection efficiencies for each density, as well as the slightly different potential decay path lengths for the K and π. The absorption length in Cu is taken to be 15 cm when calculating the potential π and K flight path. We also assumed a 10^{-3} pion punchthrough probability which is our estimate of the total probability for a pion to fake a muon by all the possible mechanisms. Based on a previous experiment[26] with this apparatus, we believe this estimate to be good to a factor of 2. The fact that this probability can only be estimated with a large uncertainty is not too important since it only contributes about 10% to the total "decay" process. The raw and corrected numbers are shown in Table VIa. The K decays with like sign muons are most likely to be 2 K_L^o decays accidentally in time.

Using now the flux, as determined above, we can calculate the number of events for each density where either both decays occur after the Q counter, or the K_L^o decays after the Q counter and the π manages to penetrate through the Cu block. The pion penetration accounts now for 50% of these events at high density and 34% at low density, so this background calculation is quite a bit more sensitive to the pion penetration level. The calculated numbers of these events are shown in Table VIIb.

B. <u>ω Decays</u>

To estimate the number of potential $\mu^+\mu^-$ pairs originating from $\omega \to \pi^o \mu^+\mu^-$ decays we have used the following input:[27]

i) $R = \dfrac{\omega \to \pi^o\mu^+\mu^-}{\omega \to \mu^+\mu^-} = 0.64$,

ii) one quarter of all high mass di-muon events are due to ω's,

iii) the relative efficiency for detection $\omega \to \pi^o\mu^+\mu^-$ to $\omega \to \mu^+\mu^-$ as calculated by Monte Carlo is 0.5.

The calculated numbers for each density are shown in Table VIIc.

C. <u>η Decays</u>

The best theoretical estimates give[28]

$$\frac{\eta \to \mu^+\mu^-\gamma}{\eta \to \text{all}} = 2.85 \times 10^{-4} .$$

Combined with the experimental measurement of[29]

$$\frac{\eta \to \mu^+\mu^-}{\eta \to \text{all}} = (2.2 \pm 0.8) \times 10^{-5}$$

and the relative Monte Carlo detection efficiency of 2.5 in favor of the 2-body decay, this leads to the conclusion that we should see about 5 $\eta \to \mu^+\mu^-\gamma$ events for every $\eta \to \mu^+\mu^-$. Even though no $\eta \to \mu^+\mu^-$ peak exists in our data, we could not exclude the existence of 15-20 events of this type, or 75-100 events from $\eta \to \mu^+\mu^-\gamma$, enough to explain the remaining low mass events. It remains to ask what that would imply about the total η production rate. Again on the basis of our Monte Carlo calculation and assuming that

$$B_{\rho\to 2\mu}\ \sigma_\rho = B_{\omega\to 2\mu}\ \sigma_\omega = \frac{1}{2}\ B_{\phi\to 2\mu}\ \sigma_\phi,$$

this would imply that η's are produced at a rate comparable to that of the ω mesons. We know of no data which either supports or contradicts this kind of production rate. We can only note for reference that in K^-p interactions at lower energies the exclusive ω production channels tend to be a factor of 3-5 or so higher than the corresponding η channels.[30]

D. Bethe-Heitler Processes

We should consider here two sources of parent γ rays which then could convert to $\mu^+\mu^-$ pairs, namely γ rays from π^o's arising from $K_L^o \to 3\pi^o$ decays, and γ rays from π^o's produced in K_L^o-Cu interactions. The first source has been shown to be completely negligible (<0.1 event) based on Monte Carlo studies. To estimate the second source of potential background, we start by assuming that the x and P_T distributions for the inclusive π^o production by K_L^o's in our energy range is the same as that of π^-'s in K^-p interactions at 32 GeV/c.[31] This is probably not a bad assumption, since the charges of the pions in both cases correspond to the charge of the incoming K, and the K^- energy is only a factor of 2 above our peak energy. Furthermore, we take the average π^o multiplicity to be 1.6, as quoted in Ref. 31. Combining this with the probability that a γ converts to a $\mu^+\mu^-$ pair as calculated by Tsai,[32] we arrive at the contributions due to the Bethe-Heitler process indicated in Table VIId. On the other hand, if we use the x and P_T distributions as given in equation V.1, we arrive at the Bethe-Heitler contributions shown in Table VIIe. Thus the Bethe-Heitler contributions to the low mass events is highly uncertain due to its high sensitivity to the production dynamics in the high x region for $K^oN \to \pi^o X$.

IX. CONCLUSION

Muon pairs have been observed in K_L^o interactions and they appear to fall into two categories: low mass ($m_{\mu\mu} < 0.5$ GeV/c^2) and high mass ($m_{\mu\mu} > 0.5$ GeV/c^2) corresponding to vector meson decays. Using reasonably orthodox assumptions it appears that there is no need to invoke any new sources to explain the low mass pairs. Alternatively, if one tries to add up the minimum required contributions to the low mass muon pairs from the known sources, e.g. K decays, ω radiative decays, and Bethe-Heitler processes, we can set an upper limit on the production cross section of new-source low mass muon pairs of 90 nb. In deriving this upper limit we have used our Bethe-Heitler calculation from Table VIIe, taken the η production cross section to be negligible, and assumed that the production cross section for μ pairs has the same A dependence as the total K_L^o cross section.

Our resolution is not good enough to resolve the three neighbouring vector mesons, ρ, ω, and ϕ. The mass spectrum is fitted well by assuming that

$$B_{\rho\to 2\mu}\ \sigma_\rho = B_{\omega\to 2\mu}\ \sigma_\omega = \frac{1}{2}\, B_{\phi\to 2\mu}\ \sigma_\phi \ ,$$

where $B_{V\to 2_\mu}$ is the branching ratio of a given vector meson into muon pairs, and σ_V the production cross section of that vector meson integrated over our K_L^o spectrum.[33] The assumed production angular distribution

$$\frac{d\sigma}{dx dP_T^2} \alpha (1 - |x|)^3 e^{-4.2P_T^2}$$

appears to fit the data reasonably well. The total cross section per nucleon for high mass $\mu\mu$ pair production turns out then to be 2.4 mb. Again, we assume the same A dependence for $\mu\mu$ pair production as for the total K^o cross section.

Even though our acceptance (see Fig. 5) is falling off fast with the increasing mass once one goes beyond 1.5 GeV, we still retain some sensitivity even at the ψ mass of 3.1 GeV. No events were observed in this vicinity. Averaged over our K_L^o momentum spectrum, this gives an upper limit on $B_{\psi\to 2\mu}\,\sigma_\psi$ of 0.2 μb at a 90% confidence level. The same production model was used in deriving this upper limit as was used for lower mass vector mesons.

Acknowledgments

We thank R. Coombes, D. Hitlin, D. Porat, and C. Rasmussen for their contributions to this experiment. We also acknowledge the excellent support of the Accelerator Operations, Experimental Facilities, and Computer Operations groups of the Stanford Linear Accelerator Center.

REFERENCES

1. L.M. Lederman et al. PRL 25, 1923 (1970)
2. R.C. Lamb et al., PRL 15, 800 (1965); R. Burns et al., PRL 15, 830 (1963)
3. Y. Yamaguchi, Nuovo Cimento 43, 193 (1966)
4. S.D. Drell and T.M. Yan, PRL 25, 316 (1970)
5. J.P. Baymond et al., PRL 33, 112 (1974); J.A. Appel et al. PRL 33, 722 (1974); D. Bintinger et al., PRL 35, 72 (1975)
6. J.J. Aubert et al., PRL 33, 1404 (1974); J.E. Augustin et al., PRL 33, 1406 (1974)
7. G.S. Abrams et al., PRL 33, 1453 (1974)
8. H.D. Snyder et al., PRL 36, 1415 (1976); M. Binkley et al., PRL 37, 574 (1976)
9. G.S. Abrams et al., PRL 33, 1453 (1974)
10. W.C. Carithers et al., PRL 30, 1336 (1973)
11. G.R. Farrar and S.C. Frautschi, PRL 36, 1017 (1976)
12. H. Kesha et al., PRL 36, 1007, (1976); K.J. Anderson et al., PRL 37, 803 (1976)
13. B.A. Dolgoshein, "Direct Production of Muons by Protons at 35, 50, 70 GeV", paper presented at the 1976 International Conference on High Energy Physics in Tbilisi, USSR.
14. L. Leipuner et al., PRL 36, 1011 (1976); M.J. Lauterbach et al., PRL 37, 1436(C) (1976)
15. N.Z. Anisimove et al., PL 65B, 85 (1976)
16. L.B. Leipuner et al., 35, 1613 (1975); D. Bucholtz et al., PRL 36, 932 (1976)
17. L.B. Leipuner et al., 34, 103 (1975); K. Winter, PL 57B, 479 (1975)

18. see for example D. Hitlin, "New Particle Production," Proceedings of Summer Institute on Particle Physics, Nov. 1976, SLAC-198; L.M. Lederman, "Lepton Production in Hadron Collisions," Phys. Reports 26C, 149 (1976).

19. L. Baum et al., PL 60B, 485 (1976)

20. E. Beier et al., PRL 37, 1117 (1976); A. Browman et al., PRL 37, 246 (1976)

21. G. Goldhaber et al., PRL 37, 255 (1976)

22. A. Benvenuti et al., PRL 34, 419 (1975) and 35, 1199 (1975); B.C. Barish et al., PRL 36, 939 (1976); J. van Krogh et al., PRL 36, 710 (1976)

23. W. Braunschweig et al., Phys. Letters 63B, 471 (1976)

24. D. Bintinger et al., PRL 37, 732 (1976); M.A. Abolins et al., PRL 37, 417 (1976)

25. L. Eyges, Phys. Rev. 74, 1534 (1948)

26. G. Donaldson et al., Phys. Rev. D9, 2960 (1974)

27. C.H. Lai and C. Quigg have estimated the relative branching ratio $\Gamma(\omega \to \pi^o\mu^+\mu^-)/\Gamma(\omega \to \pi^o\gamma)$ as 5.5 Quoted in K.J. Anderson et al., PRL 37, 799 (1976)

28. C. Jarlskog and H. Pilkuhn, Nucl. Phys. B1, 264 (1976)

29. B.D. Hyams et al., Phys. Lett. 29B, 128 (1969)

30. J. Mott et al., PR 177, 1966 (1969); Birmingham-Glasgow-London (I.C.) Oxford-Rutherford Collaboration, PR 152, 1148 (1966)

31. M. Faccini et al., Saclay Preprint (1977), unpublished

32. Y.S. Tsai, private communication. Also see Rev. Mod. Phys. 46, No. 4, 815 (1974)

33. A similar result has been obtained in K^-Be interactions at 42 GeV/c by Y.M. Antipov et al., paper presented at the 1976 International Conference on High Energy Physics in Tbilisi, USSR.

Table 1

Event Candidates Before VEND Cut

	Interaction	K Decay	Upstream
+ -	993	1949	5126
++/--	230	91	217

Table II

Event Candidates After VEND Cut

	Interaction	K Decay	Upstream
+ -	705	1908	5035
++/--	116	81	206

Table III

Background Subtraction

		Low Mass $m_{\mu\mu} < 0.44$ GeV/c^2			High Mass $m_{\mu\mu} > 0.44$ GeV/c^2		
		0cm	4cm	8cm	0cm	4cm	8cm
(a)	Interaction events with RS, after VEND cut	131	116	82	120	91	68
(b)	+ - background from $\overline{\text{RS}}$ data	34.3	17.1	17.3	8.1	3.7	2.6
(c)	From ++/-- background	41.4	21.1	21.3	16.5	32.4	33.9
(d)	Residual signal	55.3	77.8	43.4	95.4	54.9	31.5

Table IV

Relative Rates of + −, ++, −− $\mu\mu$ Pairs

	+ −	+ +	− −
3-Body Final State	1	0	0
4-Body Final State	13	2	2

Table V

P, Q, R, S Inefficiency

	P	Q	R	S	$\overline{PQ}$ RS
Inefficiency	5.1%	2.9%	3.3%	1.8%	0.015%

Table VI

K Decay Normalization

	N_{+-}	$N_{++/--}$	$N=N_{+-}-N_{++/--}$	Relative Detection Efficiency	Relative Decay Efficiency	Corrected N
0cm	700	37	663	1.0	1.0	633
4cm	519	20	499	0.889	0.927	608
8cm	439	19	420	0.833	0.853	592

Table VII

Calculated Sources of Low Mass Di-Muons

	0cm	4cm	8cm
(a) Low Mass Signal	55.3	77.8	43.4
(b) K Decays	10.6	15.7	22.4
(c) ω Decay	6.0	4.2	3.9
(d) Bethe-Heitler I	73	51	48
(e) Bethe-Heitler II	13	9	9

The contribution from $\eta \to \mu^+\mu^-\gamma$ is discussed in Section VIIIc.

Figure Captions

1. Plan view of apparatus.
2. The incident K_L^o momentum spectrum at the Cu target.
3. Distribution of d^2, the square of the distance of closest approach for K decay events. The Monte Carlo distribution is shown for comparison.
4. Distribution of (a) muon momentum in the laboratory, (b) transverse momentum of muon, and (c) transverse momentum of $\mu^+\mu^-$ pair for interaction events. The smooth line in each case denotes the expected distribution from Monte Carlo studies.
5. Detection efficiency of the apparatus as a function of di-muon mass produced in the reaction $K_L^o N \rightarrow \mu^+\mu^- X$, integrated over the K_L^o momentum spectrum.
6. Distribution in Z for (a) interaction vertices, (b) K decay vertices, and (c) upstream vertices. The locations of the front counter banks are shown. The slashed area represents the events which are eliminated by the VEND cut. The Monte Carlo distribution for (b) is also shown.
7. Distribution in Δ TOF between the two muons for (a) + - interaction (b) ++/-- interaction, (c) + - K decay/upstream, and (d) ++/-- K decay/upstream data before background subtractions.
8. The yield of interaction events, after correction for detection efficiency and normalized to the K_L^o flux, is shown as a function of target density $1/\rho$, for (a) low mass + -, (b) high mass + -, (c) low mass ++/--, and (d) high mass ++/-- di-muon pairs. Also shown in each plot is the curve $1/\rho^2$.
9. Mass of $\mu^+\mu^-$ plotted in 0.4 GeV/c^2 bins after the VEND cut. The slashed data represent the calculated background subtraction as discussed in

Section VI. The remaining events represent our final data sample before corrections for low mass events as discussed in Section VIII.

10. Distribution in $r/\sigma(r)$ for (a) high mass interaction events, (b) K decays, both upstream and downstream of V, (c) interaction events from $\overline{RS}$ data, and (d) low mass interaction events. r is the distance between the projected and measured points in the muon WSC's. The last bin includes overflows. Backgrounds have been subtracted from plots (a), (b), and (d).

11. Distribution in Δ TOF between the 2 muons for (a) high mass interaction events, (b) K decays, both upstream and downstream of V, and (c) low mass interaction events. Backgrounds have been subtracted.

12. (a) Resolution for ρ, ω, ϕ production, (b) observed $m_{\mu\mu}$ spectrum for $K^o_{\mu 3}$ decays followed by $\pi \to \mu\nu$ together with the expected Monte Carlo distribution, (c) observed high mass di-muon spectrum and fits for various mixtures of ρ, ω, and ϕ.

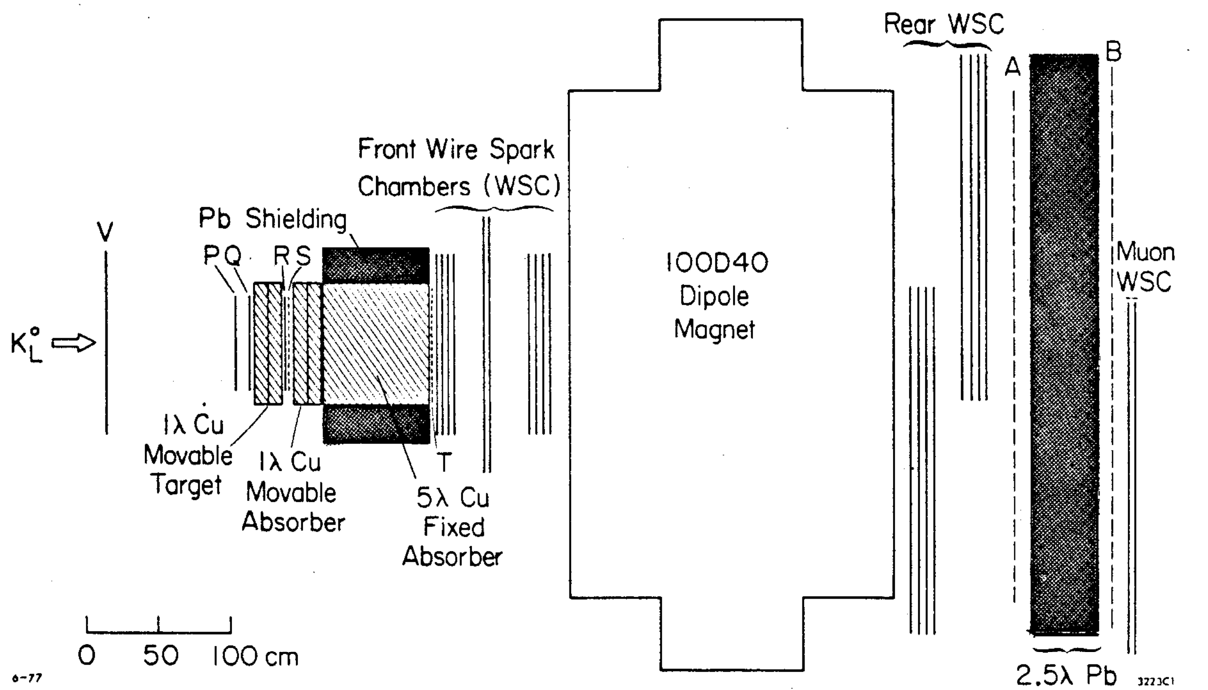
Rear WSC
A
B
Front Wire Spark
Chambers (WSC)
Pb Shielding
V
P Q
R S
100D40
Dipole
Magnet
Muon
WSC
K_L°
1λ Cu
Movable
Target
1λ Cu
Movable
Absorber
T
5λ Cu
Fixed
Absorber
0 50 100 cm
6-77
2.5λ Pb
3223C1

Fig. 1

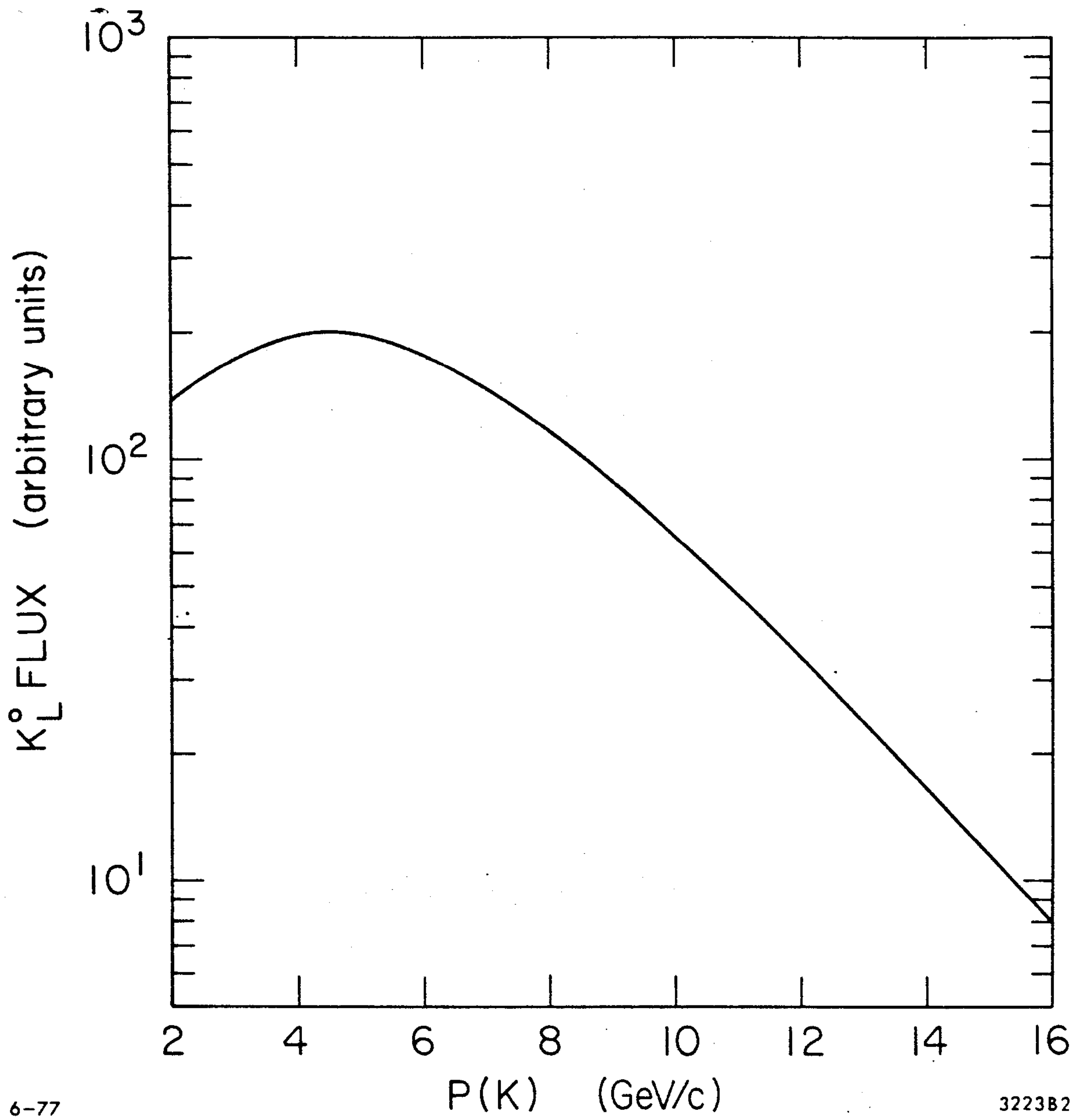
10^3
10^2
10^1
K_L^0 FLUX (arbitrary units)
2
4
6
8
10
12
14
16
P(K) (GeV/c)
6-77
3223B2

Fig. 2

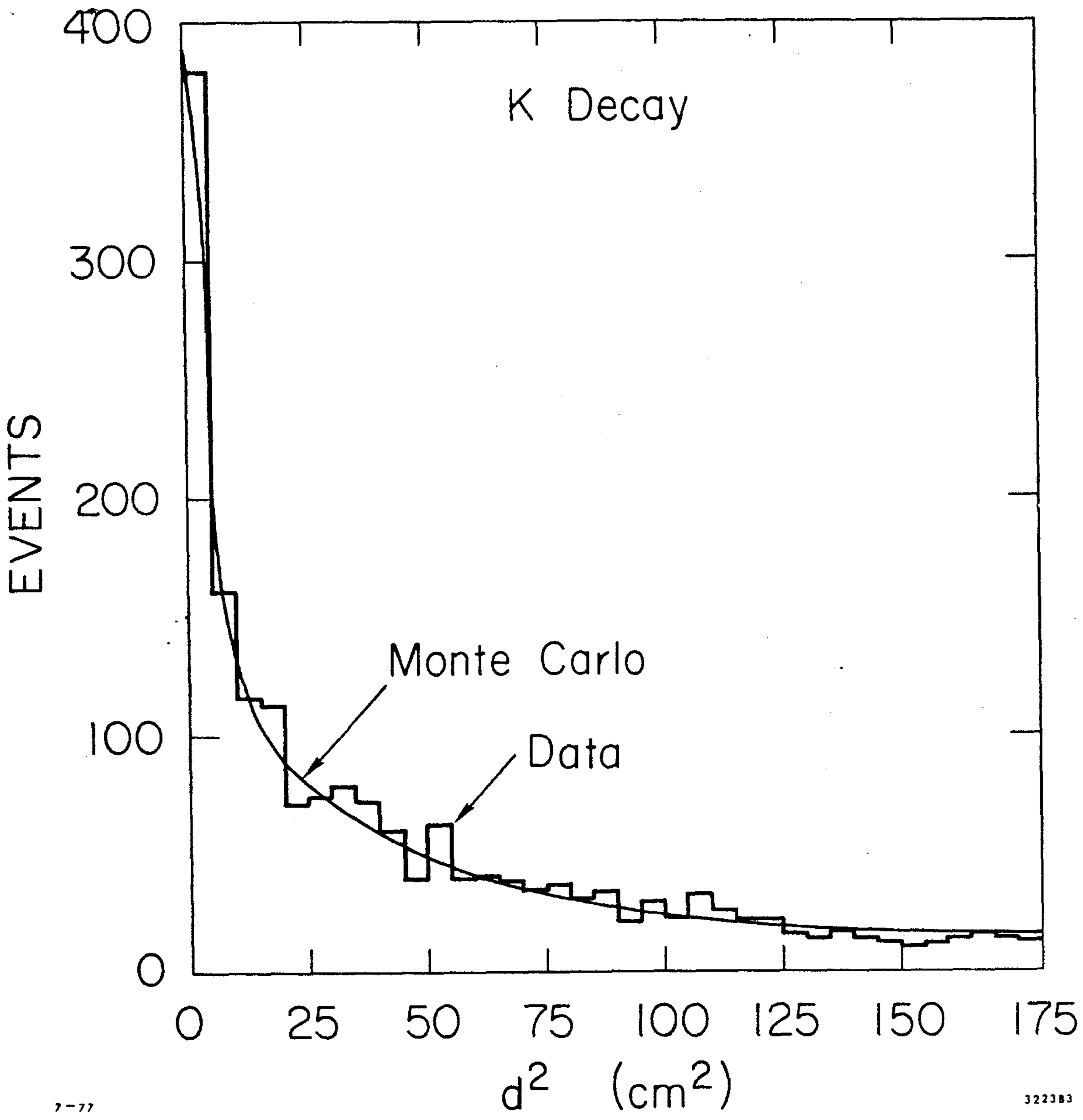
K Decay
Monte Carlo
Data
EVENTS
400
300
200
100
0
0
25
50
75
100
125
150
175
d^2 (cm^2)
7-77
3223B3

Fig. 3

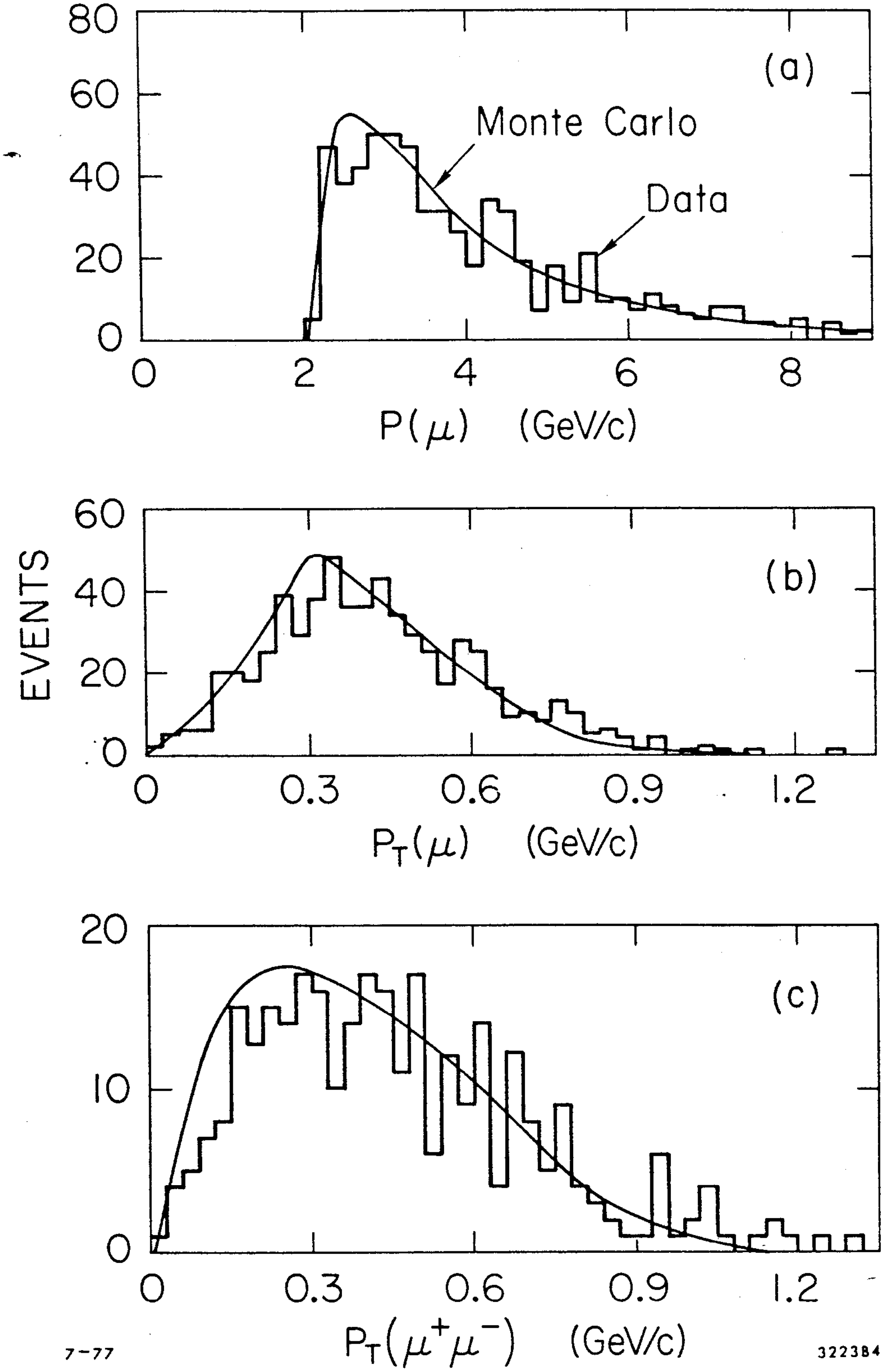
(a)
Monte Carlo
Data
80
60
40
20
0
0
2
4
6
8
$P(\mu)$ (GeV/c)
EVENTS
(b)
60
40
20
0
0
0.3
0.6
0.9
1.2
$P_T(\mu)$ (GeV/c)
(c)
20
10
0
0
0.3
0.6
0.9
1.2
$P_T(\mu^+\mu^-)$ (GeV/c)
7-77
322384

Fig. 4

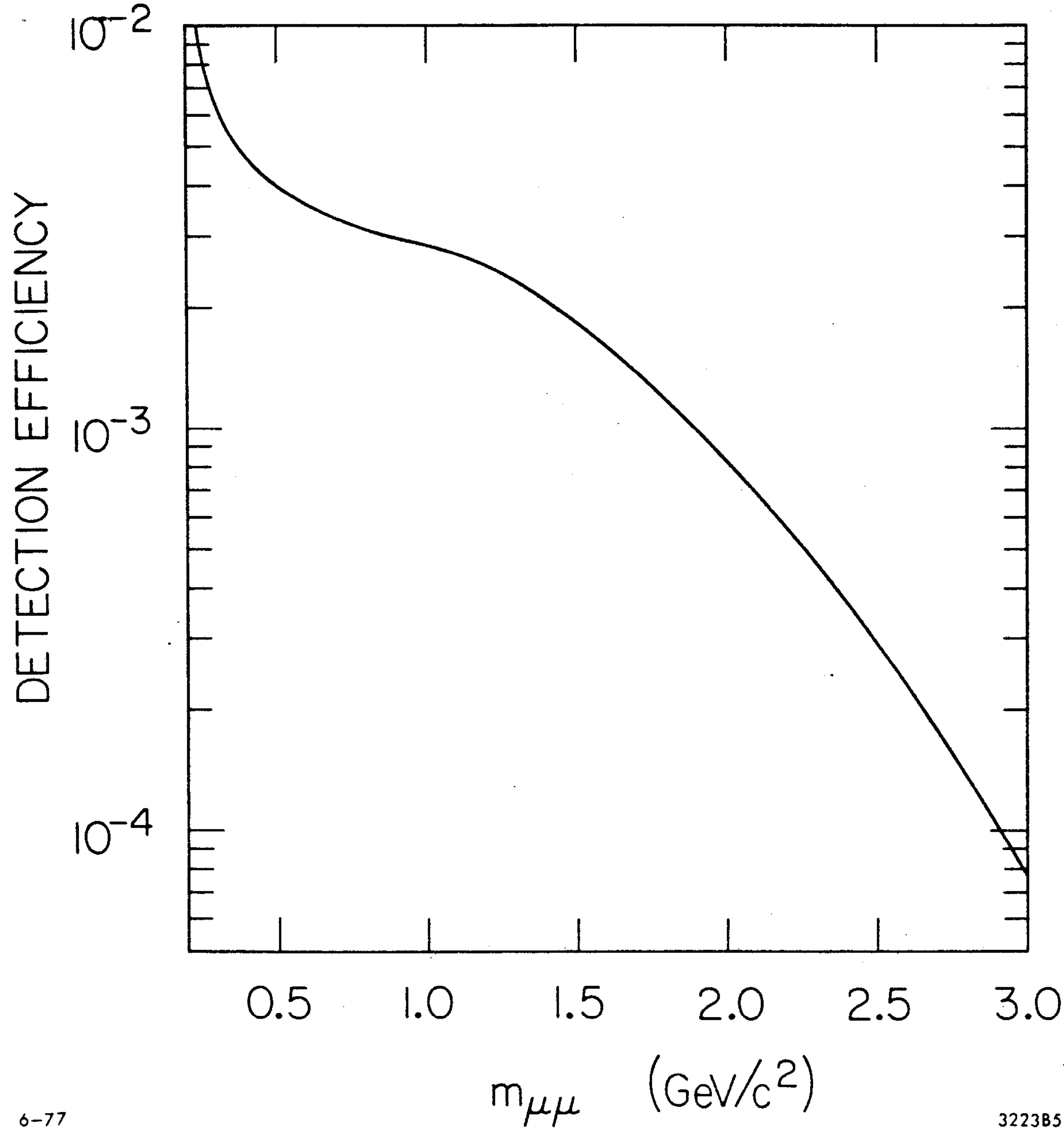

DETECTION EFFICIENCY
10^{-2}
10^{-3}
10^{-4}
0.5
1.0
1.5
2.0
2.5
3.0
$m_{\mu\mu}$ (GeV/c^2)
6-77
3223B5

Fig. 5

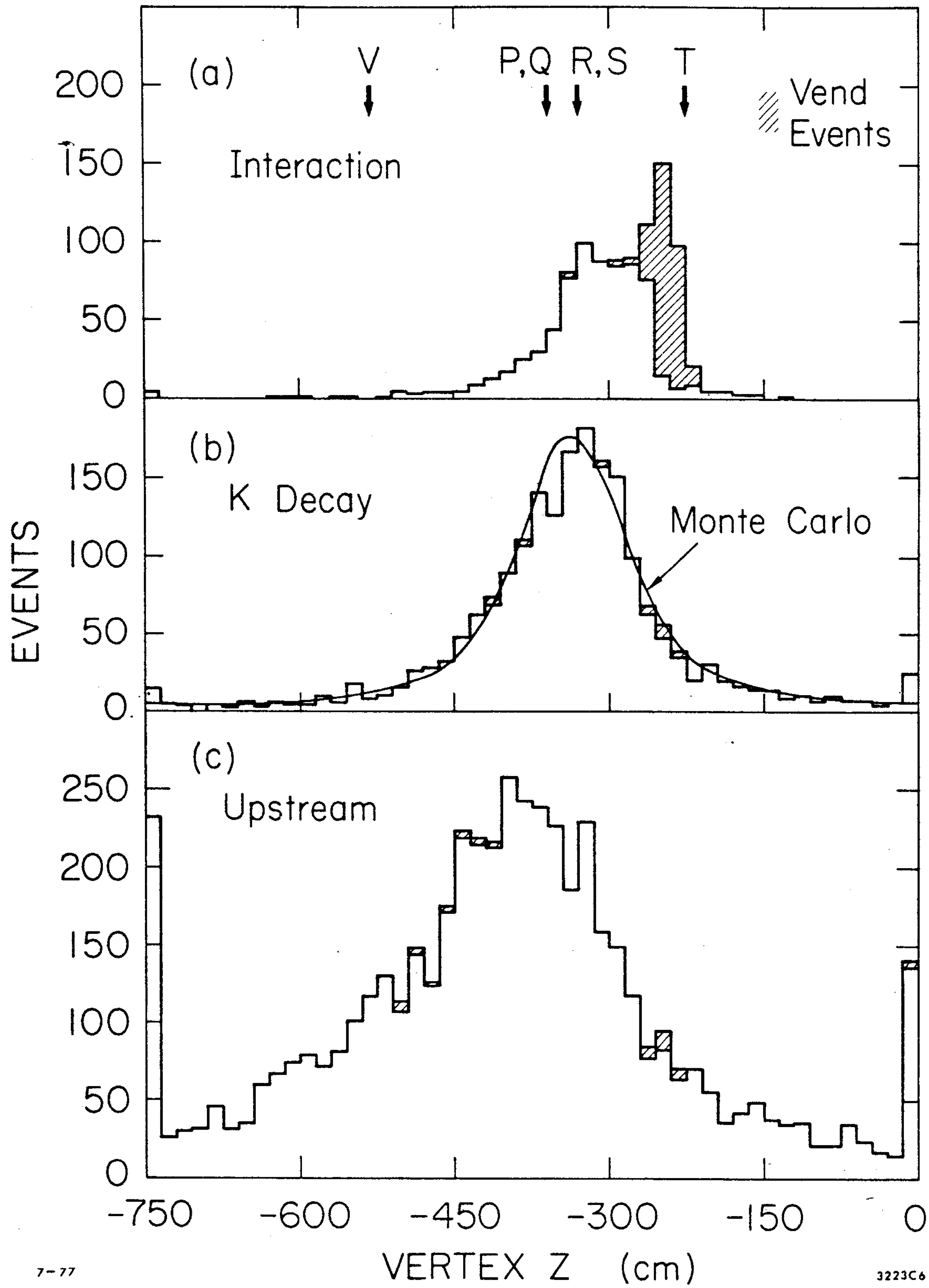
(a)
V
P,Q
R,S
T
Vend Events
Interaction
(b)
K Decay
Monte Carlo
(c)
Upstream
EVENTS
200
150
100
50
0
150
100
50
0
250
200
150
100
50
0
-750
-600
-450
-300
-150
0
VERTEX Z (cm)
7-77
3223C6

Fig. 6

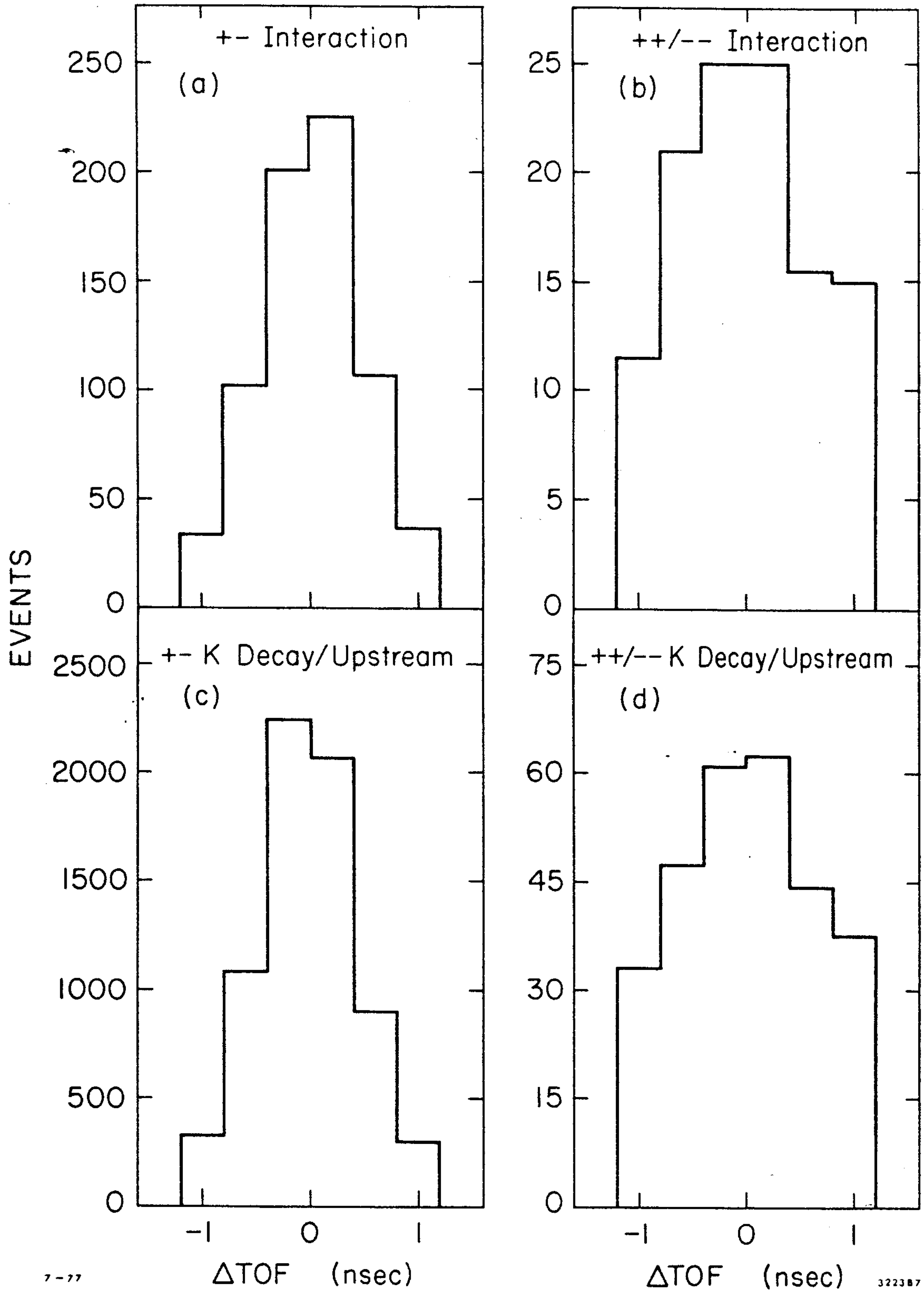

+− Interaction
(a)
++/−− Interaction
(b)
+− K Decay/Upstream
(c)
++/−− K Decay/Upstream
(d)
EVENTS
250
200
150
100
50
0
2500
2000
1500
1000
500
25
20
15
10
5
75
60
45
30
15
−1
0
1
ΔTOF (nsec)
7-77
322387

Fig. 7

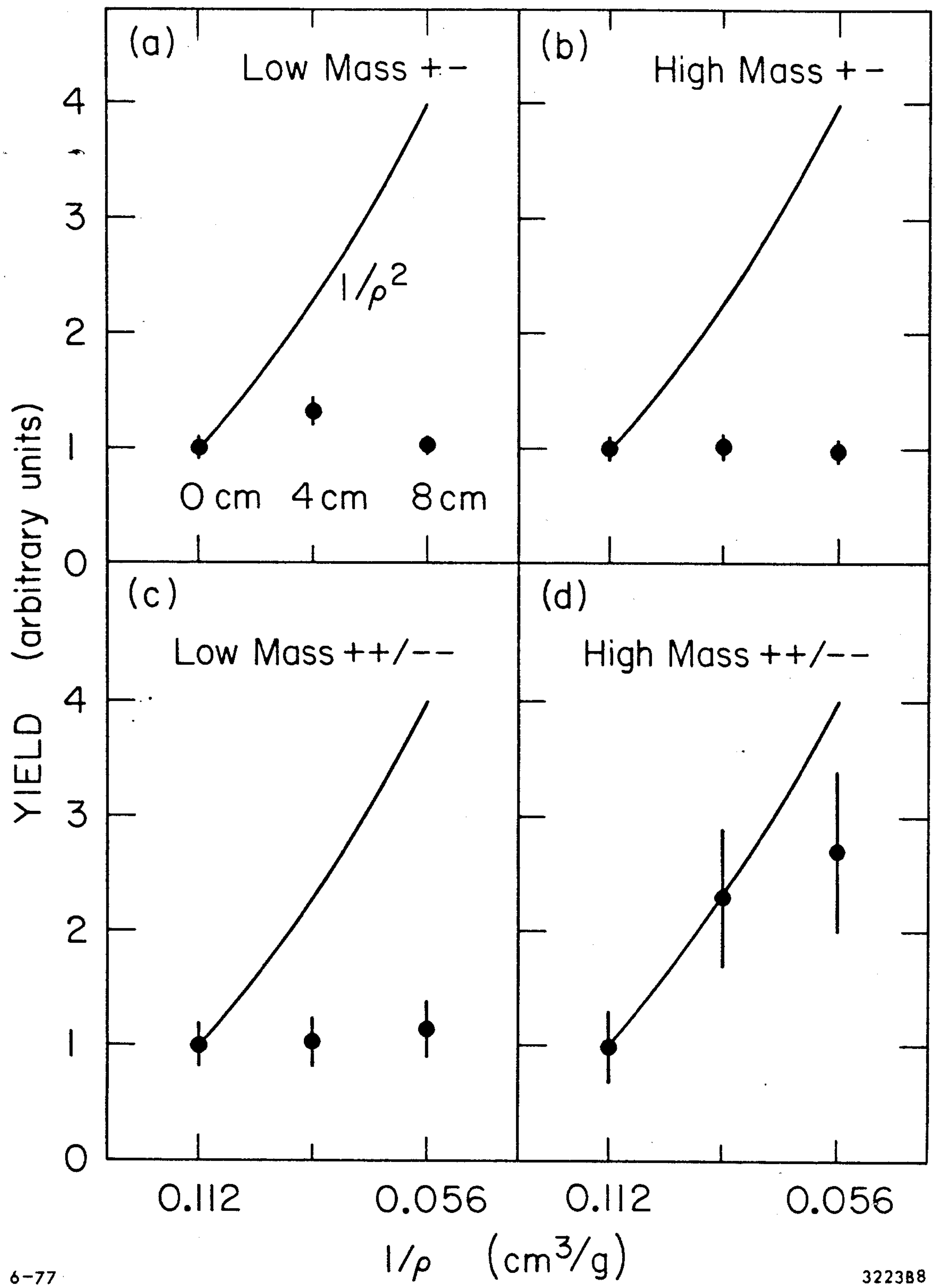
(a)
Low Mass +-
(b)
High Mass +-
(c)
Low Mass ++/--
(d)
High Mass ++/--
1/ρ²
0 cm
4 cm
8 cm
YIELD (arbitrary units)
0
1
2
3
4
0.112
0.056
1/ρ (cm³/g)
6-77
3223B8

Fig. 8

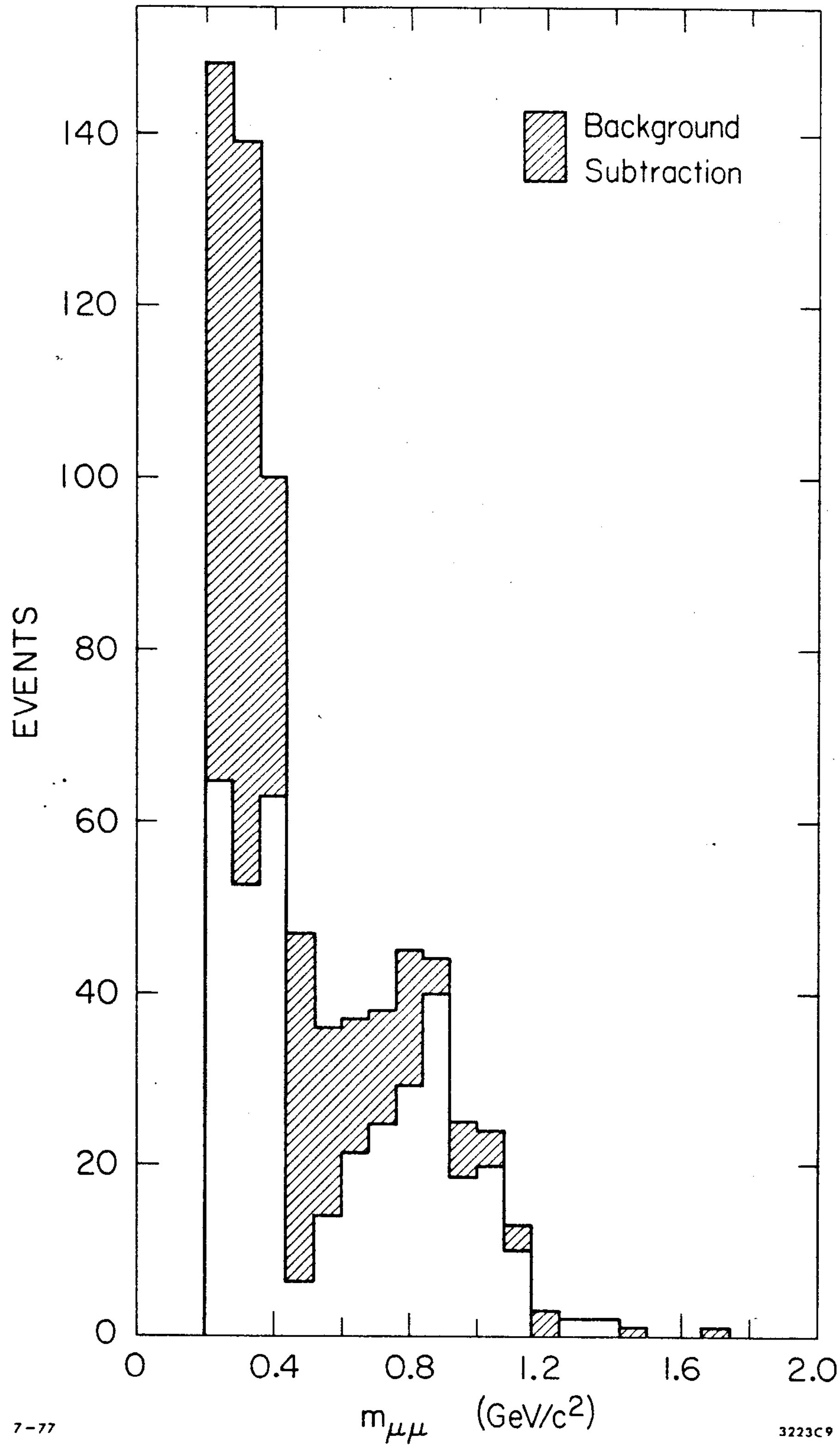

Background Subtraction
EVENTS
140
120
100
80
60
40
20
0
0
0.4
0.8
1.2
1.6
2.0
$m_{\mu\mu}$ (GeV/c^2)
7-77
3223C9

Fig. 9

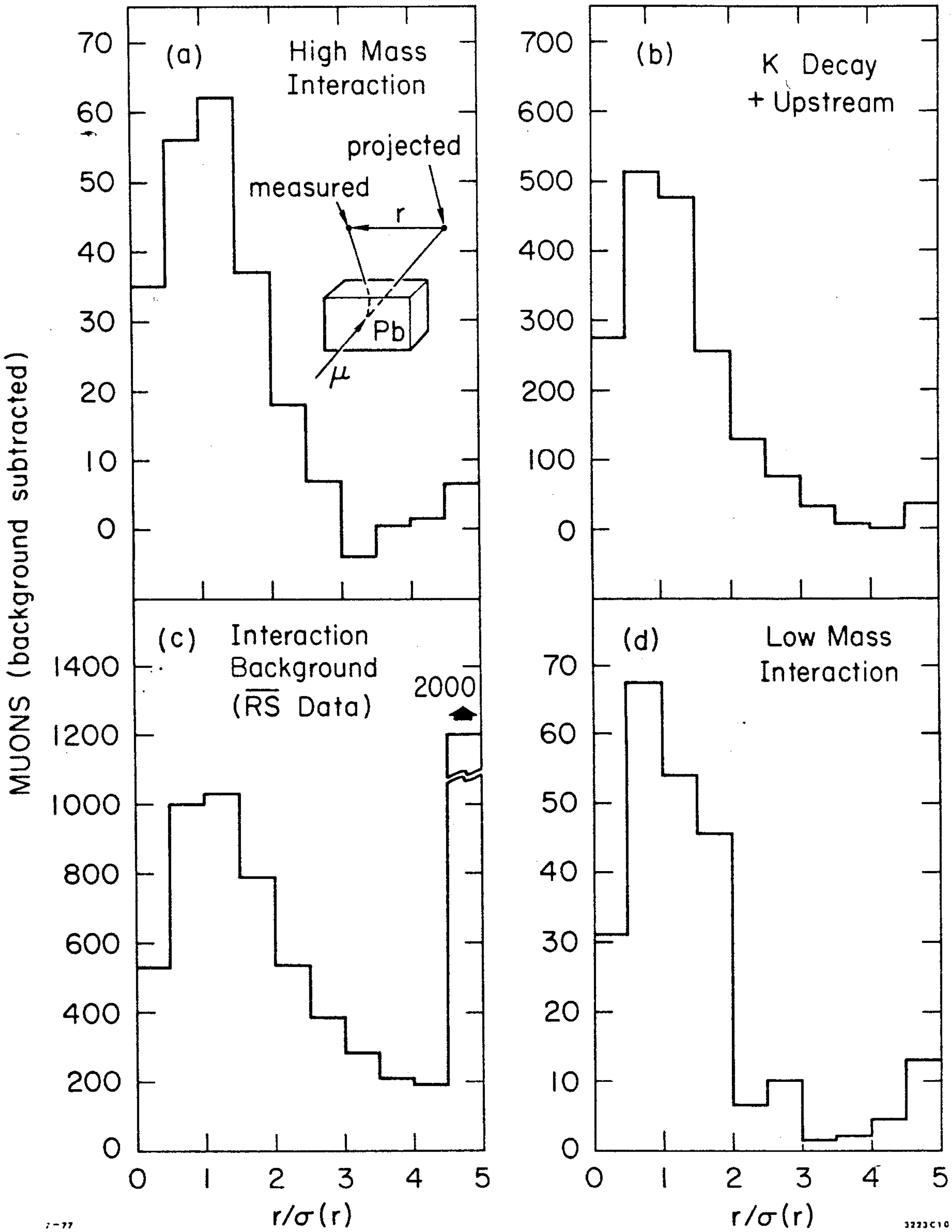

(a) High Mass Interaction
projected
measured
r
Pb
μ
(b) K Decay + Upstream
(c) Interaction Background ($\overline{RS}$ Data)
2000
(d) Low Mass Interaction
MUONS (background subtracted)
r/σ(r)
r/σ(r)

Fig. 10

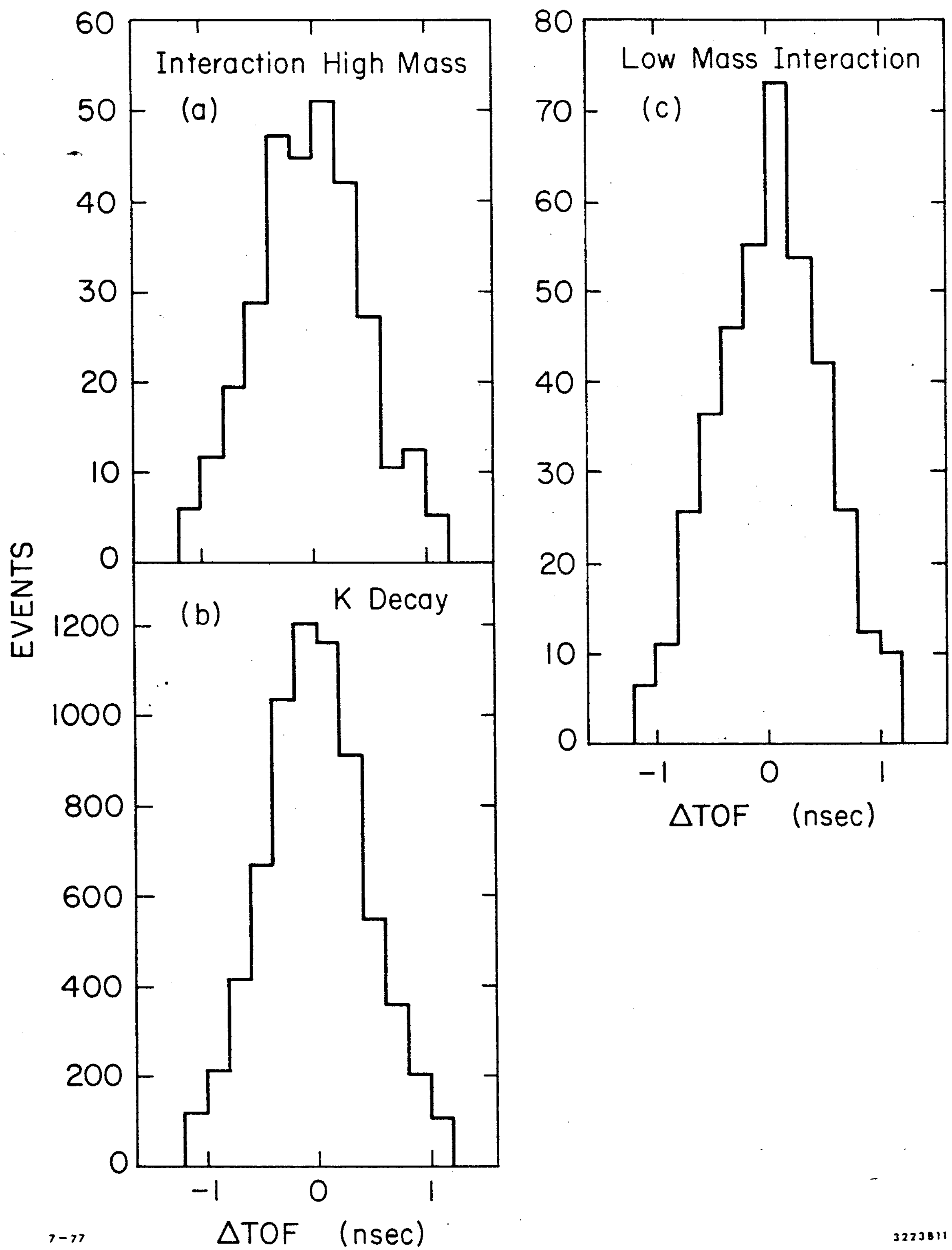
Interaction High Mass
(a)
60
50
40
30
20
10
0
EVENTS
(b)
K Decay
1200
1000
800
600
400
200
0
−1
0
1
ΔTOF (nsec)
7-77
Low Mass Interaction
(c)
80
70
60
50
40
30
20
10
0
−1
0
1
ΔTOF (nsec)
3223B11

Fig. 11

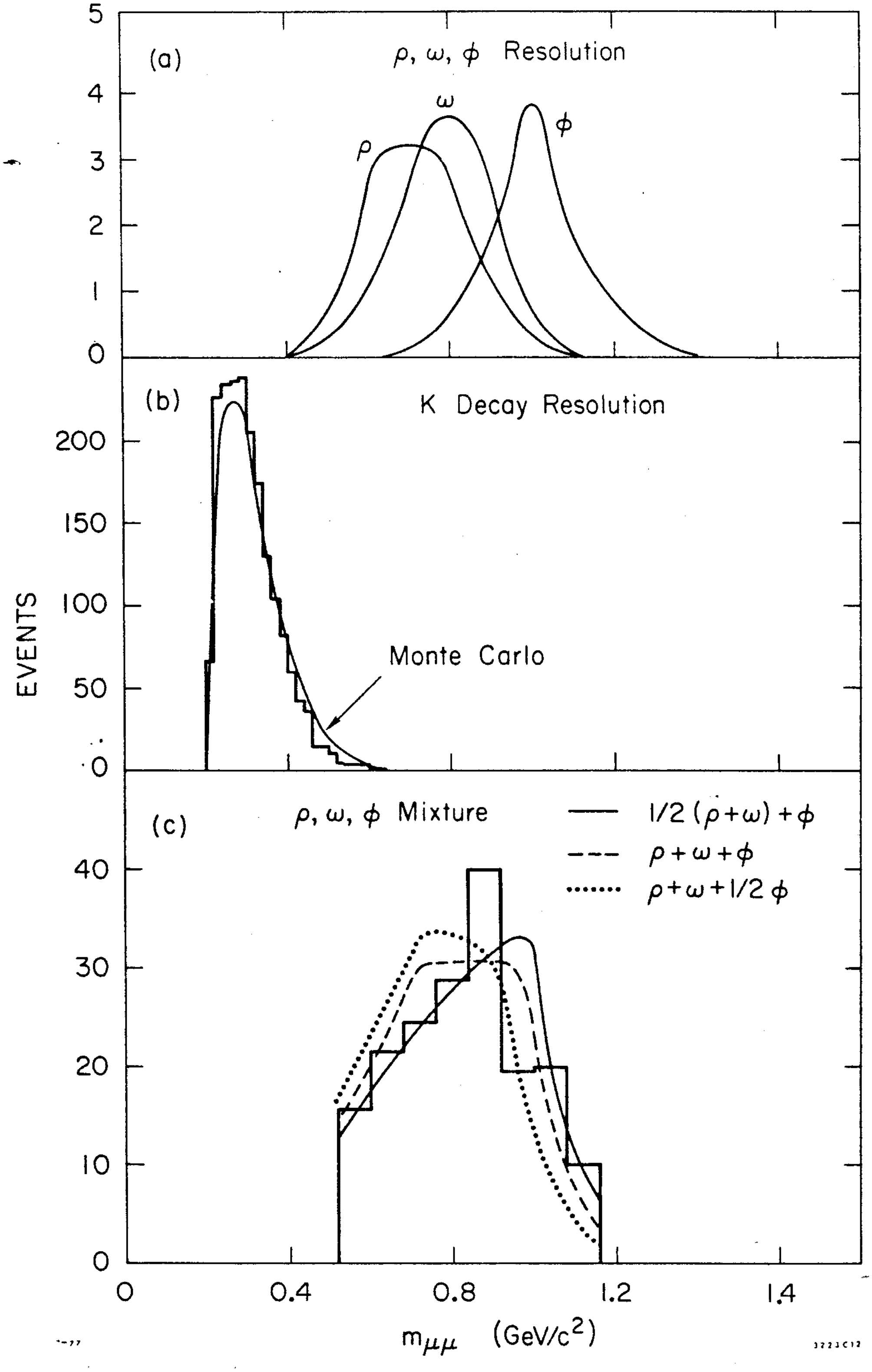

(a)
ρ, ω, φ Resolution
ρ
ω
φ
(b)
K Decay Resolution
Monte Carlo
EVENTS
(c)
ρ, ω, φ Mixture
1/2 (ρ+ω) + φ
ρ + ω + φ
ρ + ω + 1/2 φ
0
0.4
0.8
1.2
1.4
mμμ (GeV/c²)

Fig. 12